



Theory and Technology in Natural Sciences and Watershed Management

Earth Systems Institute

A **Landscape-Scale** **Landslide Model**

Documentation
of ESI's
Landscape Simulator

Copyright © 2002 Earth Systems Insitute

A Landscape-Scale Landslide Model

A Landscape Geometry for Mass Wasting	1
<i>Identification of Bedrock Hollows</i>	1
<i>Identification of landslide and debris flow runout</i>	2
Landslide Susceptibility	3
<i>Failure Model</i>	4
<i>Soil properties</i>	4
<i>Forest Cover: Root Strength and Surcharge</i>	5
<i>Slope Gradient</i>	6
<i>Soil Depth</i>	6
<i>Saturation Depth</i>	7
<i>Storms</i>	7
Calculating a Landscape-Scale, Mass-Wasting Response to Disturbance	9
<i>Setting Initial Conditions</i>	9
<i>Specifying Disturbance and Response</i>	9
References	10

A Landscape-Scale Landslide Model

Midslope landslides comprise an important component of the sediment budget in this and many other landscapes. Midslope landslides are here defined as shallow-rapid soil failures that traverse some runout length before encountering stream channels, as opposed to inner gorge landslides, which occur on steep, inner-gorge slopes directly adjacent to stream channels, and deep-seated landslides, which entail mass movement extending substantially below the rooting depth of plants. Midslope landslides initiate in bedrock hollows: downslope-oriented depressions along hillslopes into which downslope soil creep and water seepage converge. A proportion of midslope landslides initiate debris flows, a fluid slurry of sediment and water that can scour channels to bedrock. This erosive ability causes debris flows to grow as they go, and thus to create substantial deposits where they stop.

Debris flows are major players in development of the local stream environment (e.g., *Benda, 1990*). Upstream scour leaves low-order channels devoid of substrate for periods lasting decades, perhaps centuries. Downstream deposition creates fans and terraces, permanently altering stream course and bed texture. Sediment delivered can locally inundate a channel and bury riparian zones. The importance and consequences of these effects, integrated over a watershed, depend on the temporal and spatial sequence of debris flows (*Benda and Dunne, 1997*). The disturbance regime of a watershed is set in large part by the temporal and spatial patterns of debris flow occurrence and, in particular, by variations in those patterns.

Characterization of the natural disturbance regime thus requires characterization of landslide and debris flow occurrence in a way that accounts for the sequence of events over time and space; in effect, a landscape-scale landslide model. We do this using explicit, process-based numerical calculations. This involves a series of steps. 1) Define the mass-wasting geometry of the landscape: identify all potential landslide source areas – all bedrock hollows – and the runout track and points of deposition for each. 2) Define landslide susceptibility over the landscape: characterize each hollow in terms of slope stability, soil accumulation, and storm response. 3) Define the disturbance response of the landscape: monitor every hollow, year by year, fire by fire, and storm by storm.

A Landscape Geometry for Mass Wasting

Identification of Bedrock Hollows

The topographic signature of a hollow is defined in terms of slope gradient, slope curvature (the divergence in elevation, given by the Laplacian operator $\nabla^2 e$, where e = elevation), and upslope contributing area per unit contour (A/b). These values can all be estimated from the topographic representation provided by a digital elevation model (*Zevenbergen and Thorne, 1987; Tarboton, 1997*). (For these analyses all quantities are based on a DEM with 30-meter grid spacing). We calculate these quantities for all points in the DEM and identify those points having a set of values falling within some prescribed combination, similar to the strategy of *Shaw and Johnson (1995)*, but with the added factor of upslope contributing area, as described by *Montgomery and Dietrich, (1994)*.

The combination of values representative of a potentially unstable hollow is set empirically so that the spatial density (#/area) and approximate locations of such sites identified from the DEM match those estimated from examination of aerial photographs and on-ground familiarity with the area. Note that the number of *potential* landslide sites is much greater than the number of actual landslides identified in landslide inventories. Our goal here is to identify every hollow that could potentially fail at any point in time.

Identification of landslide and debris flow runout

We must also determine, for every point identified as a potential landslide site, the runout track and point(s) of deposition. This requires 1) delineation of the channel network, 2) determination of all runout paths, and 3) depositional points. The channel network is delineated from the DEM as described by *Jenson and Domingue* (1988). The upstream extent of the channel network is defined from a contributing area - slope gradient threshold described by *Montgomery and Foufoula-Georgiou* (1993), with contributing area estimated using an algorithm by *Tarboton* (1997) and slope gradient estimated using an algorithm described in *Zevenbergen and Thorne* (1987).

Landslide and debris-flow runout is determined as a function of channel gradient (*Benda and Cundy*, 1990). The grid points of the DEM do not necessarily coincide with channel locations, so channel gradient cannot be directly estimated from the elevation difference between adjacent points. Therefore channel gradient is estimated from the DEM using a polynomial fit constrained to have monotonically decreasing gradient in the downstream direction. The polynomial is fit over a moving window of variable length for all points delineated on the DEM as channels. The length of the window is a function of the estimated slope gradient: we find that a window of a kilometer or longer is required on low-gradient channels (less than a few percent), whereas a window of several hundred meters works well on high-gradient channels (more than 10%). The procedure is repeated, with the points falling below the fit line weighted preferentially (on the assumption that these grid points fall closer to the actual channel location). This procedure reproduces the channel gradients obtained from the USGS 7½-minute quadrangles (1:24000-scale topographic maps with 40-foot contours).

Debris flow deposition occurs either when channel gradient becomes less than 3.5° or at tributary junctions with junction angles exceeding 70°, as described in *Benda and Cundy* (1990). Tributary junction angles are estimated from the DEM by tracing to points 60 meters upstream along the tributary and 60 meters up and downstream from the junction point on the larger (by drainage area) channel. The junction angle is estimated from the intersection angle of the two straight-line segments (that from the upstream point on the tributary to the junction point and that from the up and downstream points on the main channel).

Using the procedures described above we thus estimate runout tracks and deposition points for every potential landslide site identified on the DEM. The empirical rules governing debris flow behavior are listed in Table 1 below.

Table 1: Bedrock Hollow ID and Debris Flow Runout
<i>Bedrock Hollows</i>
Slope Gradient $\theta > 0.6$
Divergence ($\nabla^2 e$, $e = \text{elevation}$) > 0
$\sin\theta (1 - \tan\theta)/(A/b) < 3.0$, $A/b = \text{contributing area per unit contour}$, b calculated as $b = \int \sin\phi$, where ϕ is slope aspect relative to the DEM pixel boundary. See Montgomery and Dietrich (1994) for a derivation of this equation.
<i>Debris Flow Runout</i>
A landslide entering a low-order channel of gradient less than 10° stops
A landslide entering a low-order channel of gradient greater than 10° at an intersection angle of 45° or less becomes a debris flow.
Debris flows are erosive in channels of gradient greater than 10° ; they continue downstream but start depositing material at gradients less than 10° .
At channel junctions, if the gradient of the receiving channel is less than 20° , but greater than 3.5° , a debris flow continues if the junction angle is less than 70° , otherwise it deposits on a fan.
A debris flow entering a channel of gradient greater than 20° will continue downstream, no matter what the junction angle.

Landslide Susceptibility

We characterize susceptibility to landsliding over the landscape in terms of the stability of every bedrock hollow. Stability of a hollow is a multifaceted function. It depends on the geometry of the hollow, on the depth of soil, on the vegetation cover, and on the nature of the storms that rain on it (e.g., *Hammond et al.*, 1992). Each of these factors is complex in its own right, which is why no one predicts exactly which sites will fail when. Our strategy for examining landscape response to disturbance, however, requires predicting an explicit sequence of landslide events. Clearly we cannot incorporate all the subtleties of every factor into our predictions. Rather, we use simple models that capture the primary characteristics of each (including the stochastic nature of fires and storms) and allow them to interact over thousands of simulated years. These models are described in this section.

We thus calculate explicitly which hollows fail when in the simulation. The predictions from any particular year during the simulation cannot, however, be applied directly to the landscape now. Landslide risk is a function of the sequence of events over the past centuries, which we know in the simulation, but not in reality. What we can do is to characterize each hollow in terms of its behavior over time, and the landscape in terms of the behavior of its population of hollows over time.

Failure Model

Susceptibility of the soil mantle to landsliding is estimated using the infinite slope approximation for Mohr-Coulomb limit equilibrium as described in *Benda and Dunne (1997)*. The factor of safety (ratio of shear resistance to shearing force along the slip surface) is given by

$$FS = \frac{[C_s + C_r] + [(M(\gamma_s - \gamma_w) + (1-M)\gamma_w)Z\cos^2\theta + T\cos\theta]\tan\phi}{[M\gamma_s + (1-M)\gamma_m]Z\sin\theta\cos\theta + T\sin\theta}$$

Here C_s is intrinsic cohesion of the soil and C_r the effective cohesion from roots; γ_s and γ_m are the saturated and moist specific gravity of soil, γ_w is the specific gravity of water; M is the proportion of soil saturated, which varies from 0 to 1; Z is depth of soil; θ is slope gradient; T is vegetation surcharge; and ϕ is the angle of internal friction of the soil. Soil properties (C_s , $\tan\phi$, γ_s , and γ_m) are assumed uniform in space and time; effective cohesion from roots and the weight of vegetation (T) are functions of the time since the last stand-killing fire. Slope gradient (θ) is estimated from the DEM. Given the time since the last landslide, soil depth is a function of the rate of soil accumulation, which is estimated as a function of topographic curvature determined from the DEM. The depth of saturation (M) is a function of hollow geometry, soil depth, the saturated hydraulic conductivity (K) and porosity (p) of the soil, and storm characteristics.

Soil properties

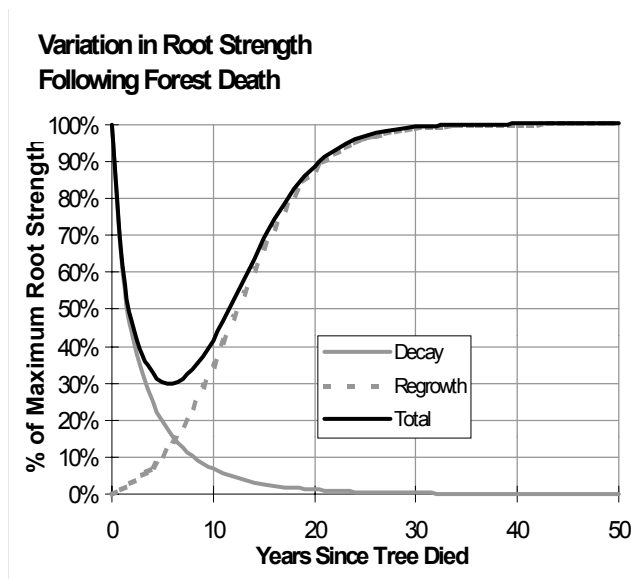
Geotechnical properties of the soil (C_s , $\tan\phi$, γ_s , γ_m , K , and p) are assumed uniform in space and time. These properties are, in fact, spatially variable, and are sometimes characterized in terms of probability distributions (e.g., *Hammond et al.*, 1992). In specifying single values for each, we ignore variability at the DEM pixel scale. Our goal at this point is to characterize the effects of topographic controls on landsliding from bedrock hollows and to see how they might vary across the landscape. Without a basis for specifying a correlation between topography and soil properties, random assignment of property values sampled from a distribution would tend to mask the effects we seek. (It is appropriate, however, to assign different soil properties to different soil and/or bedrock types.)

The colluvial soils found in the study watershed are relatively course grained with few fines (USCS type GP to GM). Sieve analysis of approximately 100 kg of soil samples ranged from 4% to 9% fines (<0.08mm) by weight, with median grain sizes (D_{50}) of 40 to 50 mm. Geotechnical values typical for such soils (e.g., *Hall et al.*, 1994) were chosen for this analysis and are listed in Table 2 below.

Table 2. Geotechnical Properties	
Cohesion	5 kPa
Friction Angle (ϕ)	35°
Moist Bulk Density	1375 kg/m ³
Saturated Bulk Density	1580 kg/m ³
Saturated Hydraulic Conductivity	1 m/hr
Porosity	0.4

Forest Cover: Root Strength and Surcharge

In this model, vegetative cover influences slope stability through the effects of root reinforcement and surcharge (the weight of trees). Roots play a primary role; surcharge a minor one. Root reinforcement is represented as a cohesion (C_r) in the factor of safety equation above. Details of the root reinforcement model are given in *Dunne* (1991) and *Benda and Dunne* (1997).



After a tree dies, roots decay with a corresponding loss of strength. Following *Sidle* (1992), the effect on C_r is represented by an exponential loss over time:

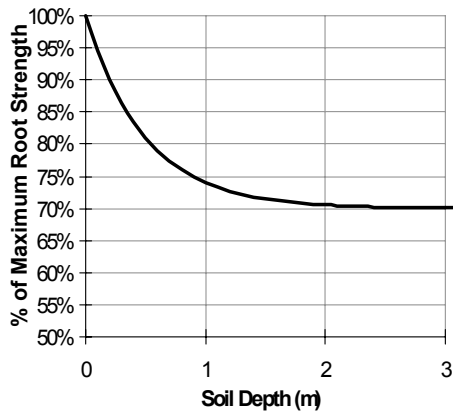
$$C_r(t) = C_r(0)\exp(-kt^n).$$

Here $C_r(t)$ is root cohesion at time t , $C_r(0)$ is root cohesion when the tree died ($t = 0$); k and n are empirical constants ($k = 0.5/\text{yr}$, $n = 0.73$). Forest regrowth and reestablishment of root strength is represented with a sigmoid curve (*Sidle*, 1992):

$$C_r(t) = C_r(0)(c + 1/[a + b\exp(-ft)]),$$

with empirical constants $a = 0.95$, $b = 19.05$, $c = -0.05$, and $f = 0.25/\text{yr}$. The combined effects of decay and regrowth are shown in the graph at right:

Variation of Root Reinforcement with Depth



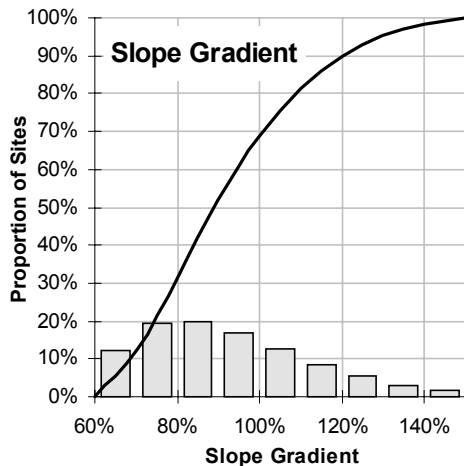
Total maximum root strength $C_r(0)$ for an old-growth conifer stand is estimated as 14 kPa (Hammond et al., 1992). Following Dunne (1991), root cohesion is partitioned between a vertical component C_{rV} , representing anchoring to bedrock, and a lateral component C_{rL} , representing the intertwined mat of roots in the soil. Thus $C_r = C_{rL} + C_{rV}$, with 70% apportioned to lateral reinforcement (C_{rL}) and 30% to vertical reinforcement (C_{rV}). The vertical component is assumed to decrease exponentially with increasing soil depth as

$$C_{rV}(Z) = C_{rV}(0)\exp(-jZ).$$

Here $C_{rV}(Z)$ is effective root cohesion at depth Z and $C_{rV}(0)$ is the maximum value of C_{rV} . A factor of minus 2 is used for j in the exponent to reflect the rooting depth of trees. Root density, and associated vertical anchoring, drops dramatically below a depth of about 1.5 meters, as shown here.

Vegetation surcharge has a very minor influence on the factor of safety. It is estimated to vary from $T = 100 \text{ kg/m}^2$ following a stand-killing fire to $T = 1000 \text{ kg/m}^2$ for stands greater than 20 years old.

Slope Gradient

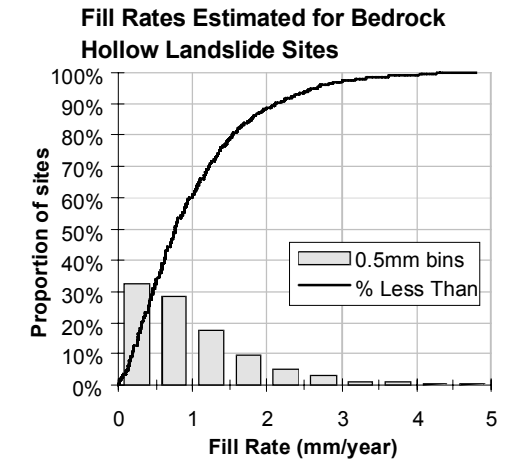


Slope gradient for each bedrock hollow is estimated from the DEM as described in *Zevenbergen and Thorne (1987)*. We find that DEM-estimated gradients are consistently a factor of about 0.7 less than gradients measured in the field. To compensate, we multiply all calculated DEM gradients by a factor of 1.4. The distribution of slope gradients estimated from the DEM for bedrock hollows in the study watershed is shown at left.

Soil Depth

Through a variety of biogenic and geomorphic processes, collectively referred to as creep, soil gradually accumulates in bedrock hollows. If the rate of creep is proportional to slope gradient, that is, $Q_s = k \cdot \tan\theta$, where Q_s is creep rate (volume per time) and θ is slope gradient, the rate of soil accumulation in a hollow is given by (see e.g., *Dietrich et al., 1995*)

$$dz/dt = k\nabla^2e$$



where z is soil depth, dz/dt is the change in soil depth with time, e is elevation of the ground surface, and ∇^2 is the Laplacian operator. Because of the similarity to the diffusion equation, k is often referred to as a diffusion coefficient. We use this equation to estimate soil accumulation in hollows. During the simulation, soil depth is calculated as $\Delta t * dz/dt$, where Δt is the time elapsed since the last landslide.

The value of $\nabla^2 e$ is determined for each hollow from the DEM. A value for k of $24 \text{ cm}^3/\text{yr}$ was estimated for the study landscape using

measurements of soil depths and surface geometry for the 6 bedrock hollows for which basal C-14 dates were obtained. The distribution of soil accumulation rates calculated for hollows in the study watershed is shown at right.

Saturation Depth

Saturation of the soil is the primary factor in triggering landslides. It is represented in the factor-of-safety equation by the value of M , the ratio of saturation depth to soil depth. The value of M is dependent on soil depth, on soil properties (porosity and hydraulic conductivity), on storm characteristics (rainfall intensity as a function of time), and on hollow geometry. Storms are characterized in terms of a duration and mean intensity, described below. The response of a hollow to any particular storm is then a complex function of storm duration and intensity, and upslope topography. We use a parameterization of hollow topography that, while maintaining the characteristics of its response to storms, greatly simplifies the calculation of saturation depth.

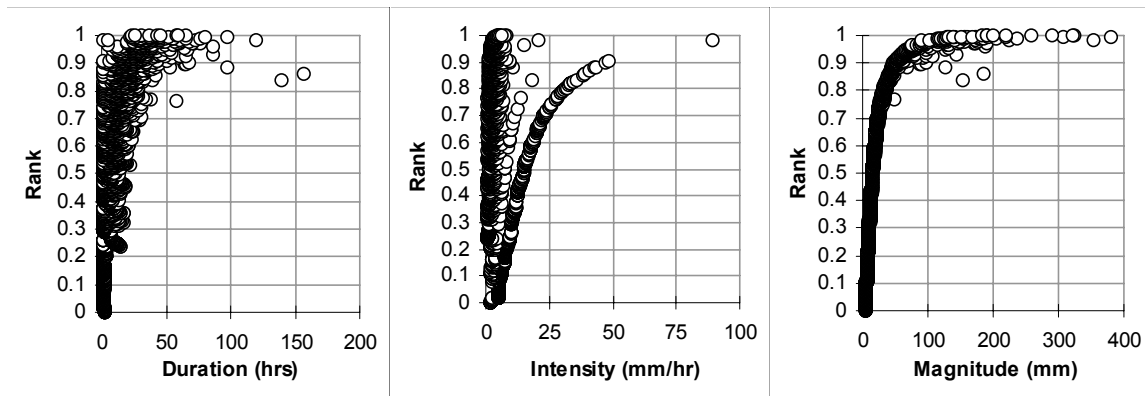
Each pixel in the DEM has associated with it a set of upstream pixels that drain to it. For each of these, a transit time for saturated subsurface flow may be estimated with Darcy's equation, if we assume that flow direction is parallel to the ground surface (e.g., *Iida*, 1984). Thus, moving upslope, we can estimate the surface area providing flow to the pixel as a function of transit time. For a given storm intensity, this effectively defines a hydrograph for subsurface flow through the pixel. This is essentially the same algorithm presented by *Maidment et al.* (1996) for surface flow, applied here to subsurface flow. With this algorithm we can define the ratio of saturation depth to soil depth as a function of storm intensity and duration for each pixel in the DEM.

Storms

It is saturated throughflow from storm rainfall that triggers landslides from bedrock hollows, so it is important that the storm climate is characterized well. Storms are characterized on the basis of empirical hourly precipitation data at Randle, Washington. Data were available for the period 1948 to 1994, at nearly 100 percent completeness. Storms were

identified from this record according to the following definition of interstorm period: continuous intervals of at least seven hours duration during which hourly precipitation totals never exceed 0.04 inches (about 1 mm). With this criteria, and after excluding events of average intensity less than 5 mm/hour, 2986 storms were identified, with an average of 79 storms per year. Each storm is characterized in terms of its duration and mean intensity.

The strategy for creating a storm climate in the simulation is to estimate the underlying probability distribution of observed storms and then to randomly sample 79 storms from this distribution each simulation year. We ranked the observed storm record in terms of the resultant factor of safety for arbitrarily selected hollows. In general, storm magnitude (the product of duration and intensity) is a better predictor for stability than either duration or intensity.



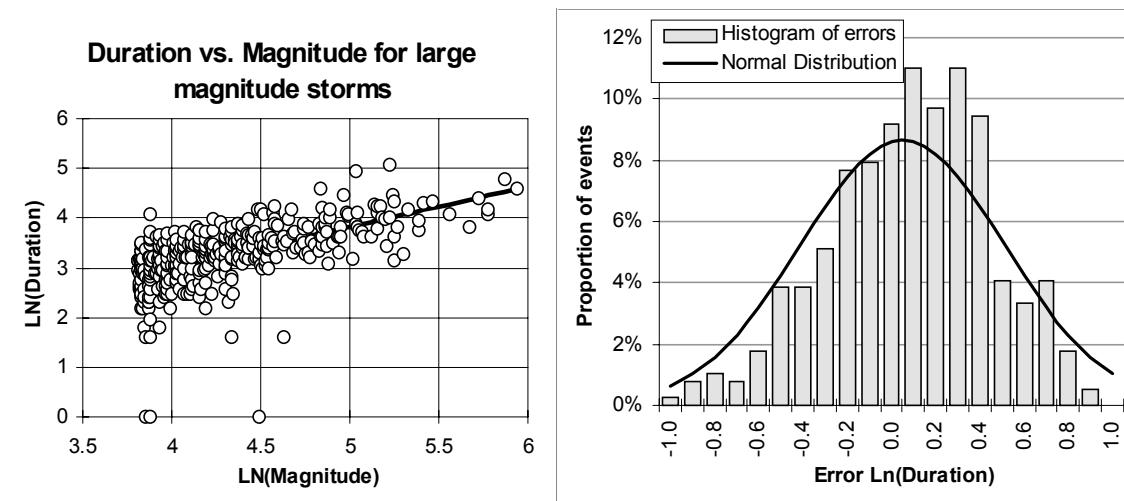
We used a two-parameter exponential function to fit the cumulative distribution of observed storm magnitudes:

$$CP_M = 1 - \exp(-M^\alpha/\beta),$$

where CP_M is the probability that a storm is of magnitude less than or equal to M ; α and β are empirical parameters ($\alpha = 0.665$, $\beta = 6.2$). It is the largest magnitude storms that trigger landslides, so the fit is preferentially weighted to the upper half of the distribution. We found that storm duration is well predicted as an exponential function of magnitude, with the log of the errors approximately normally distributed:

$$D = aM^b \exp(\sigma),$$

where D is storm duration in hours, M is storm magnitude in mm, a and b are empirical constants ($a = 0.776$, $b = 0.815$), and σ is a sample from a normal distribution with zero mean and variance of 0.46.



(We also tried correlating magnitude and intensity, but the distribution of errors was not as well behaved).

Calculating a Landscape-Scale, Mass-Wasting Response to Disturbance

The last step is to apply a disturbance regime, in terms of a sequence of fires and storms, and monitor the response of every hollow. We do this year by year, over a simulation of thousands of years, to build a set of statistics to describe the range of mass wasting conditions encountered.

Setting Initial Conditions

We must specify an initial stand age and soil depth at the start of a simulation. To create an initial distribution of stand ages, we start with a uniform age of 200 years and then run the fire model for 5000 years. To create an initial distribution of soil depths, we start with a random sample of depths from a log-normal distribution. We then run the model for 5000 years (with fires, storms, landslides, debris flows). The distribution of soil depths obtained at the end of the 5000-year initialization run is used as the starting point for the simulation.

Specifying Disturbance and Response

The factors impacting slope stability are storms and fires. Storms are estimated as described above; fires are simulated with the model described elsewhere. The DEM grid provides the spatial framework over which fires are applied and stand age monitored. We can thus specify stand age (the time since the last fire) for every hollow identified over the landscape.

We also recognize tree mortality from factors other than fire. As stands age, natural processes (disease, lightning, old age) produce an increasingly uneven distribution of tree ages within a stand. Tree death from such processes may also act to reduce root strength locally. To estimate the consequences of these factors, we used estimates of stand mortality with age to calculate a probability that the trees growing over the area of any hollow would all die in any year. This produced an additional stochastic component in the calcula-

tion of root strength, and caused a small increase in landslide rates for stands older than 100 years.

Sediment volumes in hollows and all debris-flow prone channels are monitored over time. Sediment accumulates from processes of soil creep and from landslide and debris flow deposition. We track all sources. Thus soil depth is known for each hollow each year.

Each year of the simulation the depth of soil and tree age is monitored for every hollow. The five largest magnitude storms from the sample of 79 are applied to each hollow and a factor of safety calculated. A factor of safety of less than 1 signifies a landslide. The hollow fails, and the landslide debris is routed downslope until it reaches the points of deposition. Tree age and soil depths are set to zero along the runout track.

When a landslide occurs, the volume of soil available along the landslide and debris flow track is known, so that deposit volumes can be calculated. Sediment deposited in low-order channels (e.g., at a tributary junction) may be incorporated into a future debris flow. Sediment in low-order channels is also eroded by fluvial processes over time. We assume that, averaged over time, about 20% of all sediment deposited in low-order (colluvial channels *sensu Montgomery and Buffington, 1997*) is removed by fluvial processes (*Benda, 1994; Swanson et al., 1982*). The volume eroded each year ΔV is calculated as

$$\begin{aligned}\Delta V &= -\epsilon V(T_{\max} - t), & t < T_{\max}, \\ \Delta V &= 0, & t > T_{\max},\end{aligned}$$

where T_{\max} represents the time to complete armoring of the deposit, estimated here as 20 years, V is the volume at time t , t is time since the sediment was deposited, and ϵ is set to 0.0011157 so that ΔV , integrated over time, is 20% of the total deposited.

Each year of the simulation, for each DEM channel pixel, we monitor sediment inputs from soil creep and landslide deposition, sediment outputs from landsliding, debris flow scour, and fluvial erosion. In effect, we calculate the sediment budget, year by year. This allows us to examine interactions between different disturbance processes, here storms and fires, and to estimate the full variety of potential outcomes.

References

- Benda, L., The influence of debris flows on channels and valley floors in the Oregon Coast Range, U.S.A., *Earth Surface Processes and Landforms*, 15, 457-466, 1990.
- Benda, L., Stochastic Geomorphology in a Humid Mountain Landscape, Dissertation thesis, University of Washington, Seattle, WA, 1994.
- Benda, L., and T. Dunne, Stochastic forcing of sediment supply to channel networks from landsliding and debris flow, *Water Resources Research*, 33 (12), 2849-2863, 1997.
- Benda, L.E., and T.W. Cundy, Predicting deposition of debris flows in mountain channels, *Canadian Geotechnical Journal*, 27, 409-417, 1990.

- Dietrich, W.E., R. Reiss, M.-L. Hsu, and D.R. Montgomery, A process-based model for colluvial soil depth and shallow landsliding using digital elevation data, *Hydrological Processes*, 9, 383-400, 1995.
- Dunne, T., Stochastic aspects of the relations between climate, hydrology and landform evolution, *Transactions of the Japanese Geomorphological Union*, 12, 1-24, 1991.
- Hall, D.E., M.T. Long, and M.D. Remboldt, Slope Stability Reference Guide for National Forests in the United States, pp. 321, United States Department of Agriculture, Forest Service, Washington D.C., 1994.
- Hammond, C., D. Hall, S. Miller, and P. Swetik, Level 1 Stability Analysis (LISA) Documentation for Version 2.0, United States Department of Agriculture, Forest Service, Intermountain Research Station, Ogden, Utah, 1992.
- Iida, T., A hydrological method of estimation of the topographic effect on the saturated throughflow, *Transactions of the Japanese Geomorphological Union*, 5, 1-12, 1984.
- Jenson, S.K., and J.O. Domingue, Extracting topographic structure from digital elevation data for geographic information system analysis, *Photogrammetric Engineering and Remote Sensing*, 54 (11), 1593-1600, 1988.
- Maidment, D. R., F. Olivera, A. Calver, A. Eatherall, W. Fraczek, Unit hydrograph derived from a spatially distributed velocity field, *Hydrological Processes*, (10), 831-844, 1996.
- Montgomery, D.R., and J.M. Buffington, Channel-reach morphology in mountain drainage basins, *Geological Society of America Bulletin*, 106 (5), 596-611, 1997.
- Montgomery, D.R., and W.E. Dietrich, A physically based model for the topographic control on shallow landsliding, *Water Resources Research*, 30 (4), 1153-1171, 1994.
- Montgomery, D.R., and E. Fournoula-Georgiou, Channel network source representation using digital elevation models, *Water Resources Research*, 29 (12), 3925-3934, 1993.
- Shaw, S.C., and D.H. Johnson, Slope morphology model derived from digital elevation data, in *Northwest ARC/INFO Users Conference*, Coeur d'Alene, ID, 1995.
- Sidle, R.C., A theoretical model of the effects of timber harvesting on slope stability, *Water Resources Research*, 28, 1897-1910, 1992.
- Swanson, F.J., R.L. Fredriksen, and F.M. McCorison, Material transfer in a western Oregon forested watershed, in *analysis of Coniferous Forest Ecosystems in the Western United States*, edited by R.L. Edmonds, pp. 233-266, Hutchinson Ross Publishing Co., Stroudsburg, Penn., 1982.
- Tarboton, D.G., A new method for the determination of flow directions and upslope areas in grid digital elevation models, *Water Resources Research*, 33 (2), 309-319, 1997.
- Zevenbergen, L.W., and C.R. Thorne, Quantitative analysis of land surface topography, *Earth Surface Processes and Landforms*, 12, 47-56, 1987.